

Real-space, real-time approach to quantum-electrodynamical time-dependent density functional theory

Cite as: J. Chem. Phys. **157**, 194106 (2022); <https://doi.org/10.1063/5.0123909>

Submitted: 01 September 2022 • Accepted: 04 November 2022 • Accepted Manuscript Online: 07 November 2022 • Published Online: 16 November 2022

Justin Malave,  Alexander Ahrens,  Daniel Pitagora, et al.



[View Online](#)



[Export Citation](#)



[CrossMark](#)

ARTICLES YOU MAY BE INTERESTED IN

[Advances in modeling plasmonic systems](#)

The Journal of Chemical Physics **157**, 190401 (2022); <https://doi.org/10.1063/5.0130790>

[Quantification of electron correlation for approximate quantum calculations](#)

The Journal of Chemical Physics **157**, 194101 (2022); <https://doi.org/10.1063/5.0119260>

[Virial equation of state as a new frontier for computational chemistry](#)

The Journal of Chemical Physics **157**, 190901 (2022); <https://doi.org/10.1063/5.0113730>



A smiling man in a blue shirt stands next to a stack of three silver-colored Lock-in Amplifiers. The top unit is labeled "Zurich Instruments". To the right, there is promotional text and the Zurich Instruments logo.

Time to get excited.
Lock-in Amplifiers – from DC to 8.5 GHz

[Find out more](#)

 Zurich
Instruments

Real-space, real-time approach to quantum-electrodynamical time-dependent density functional theory

Cite as: J. Chem. Phys. 157, 194106 (2022); doi: 10.1063/5.0123909

Submitted: 1 September 2022 • Accepted: 4 November 2022 •

Published Online: 16 November 2022



View Online



Export Citation



CrossMark

Justin Malave,¹ Alexander Ahrens,¹ Daniel Pitagora,¹ Cody Covington,² and Kálmán Varga^{1,a)}

AFFILIATIONS

¹ Department of Physics and Astronomy, Vanderbilt University, Nashville, Tennessee 37235, USA

² Department of Chemistry, Austin Peay State University, Clarksville, Tennessee 37044, USA

^{a)} Author to whom correspondence should be addressed: kalman.varga@vanderbilt.edu

ABSTRACT

The quantum-electrodynamical time-dependent density functional theory equations are solved by time propagating the wave function on a tensor product of a Fock-space and real-space grid. Applications for molecules in cavities show the accuracy of the approach. Examples include the coupling strength and light frequency dependence of the energies, wave functions, optical absorption spectra, and Rabi splitting magnitudes in cavities, as well as a description of high harmonic generation in cavities.

Published under an exclusive license by AIP Publishing. <https://doi.org/10.1063/5.0123909>

I. INTRODUCTION

The possibility of altering physical and chemical properties by coupling matter to light has attracted intense experimental^{1–12} and theoretical interest.^{13–59} There are several excellent review articles highlighting the present state of the art of experimental and theoretical approaches related to light-matter interaction in cavities. These include reviews about the properties of hybrid light-matter states,^{60,61} *ab initio* calculations,^{26,62} and molecular polaritonics.^{63–65}

The theoretical and computational description of the coupled light-matter system is challenging because the already difficult, quantum, many-body problem of electrons and nuclei is aggravated with the addition of the photon degrees of freedom. A plethora of approaches going beyond the simple two-level atom model⁶⁶ has been proposed in the last few years. Most of these approaches are based on successful many-body quantum methods, adopted to include photon interactions. The use of the Pauli-Fierz (PF) non-relativistic quantum electrodynamics Hamiltonian is found to be the most useful framework^{26,30,43,51,67} for practical calculations. The PF Hamiltonian is a sum of electronic and photonic Hamiltonians and a cross term describing the electron-photon interaction. Due to this cross term, one has to use a coupled electron-photon wave function

$$\sum_{\vec{n}} \Phi_{\vec{n}}(\mathbf{x}) \chi_{\vec{n}}, \quad (1.1)$$

where $\mathbf{x} = (\mathbf{r}_1, \mathbf{r}_2, \dots, \mathbf{R}_1, \mathbf{R}_2, \dots)$ are the spatial coordinates of the electrons and nuclei, and $\vec{n} = (n_1, n_2, \dots, N_p)$ are the quantum numbers of the photon modes. The occupation number basis, $\chi_{\vec{n}} = |n_1, n_2, \dots, N_p\rangle$, is used to represent the bosonic Fock-space of photon modes (see Appendix A for a more detailed definition).

Wave function based approaches^{39,68–71} typically use coupled electron-photon wave functions and the product form significantly increases the dimensionality. In Refs. 37, 39, 70, and 71, the coupled cluster (CC) approach is used, by defining a reference wave function as a direct product of a Slater determinant of Hartree-Fock states and a zero-photon photon number state. The exponentiated cluster operator acting upon this product state defines the ground state Quantum-Electrodynamical (QED)-CC wave function. Systematic improvability is the greatest benefit of this approach. The stochastic variational method^{68,69} (QED-SVM) also uses a product of matter and photonic wave functions, but in this case, the matter part is described by explicitly correlated Gaussian basis states.⁷² The parameters of the variational ansatz are optimized by a stochastic selection process leading to highly accurate energies and wave functions. Both the QED-CC and QED-SVM approaches are limited to small atoms and molecules.

A pioneering approach to describe the interaction of light and matter in cavities is the quantum-electrodynamical density functional theory (QEDFT).^{40,42,45,46,73,74} The QEDFT is an exact reformulation of the PF Hamiltonian, based many-body wave theory. In practical applications of QEDFT, one has to develop good approximations of the fields and currents so that the auxiliary non-interacting system generates the same physical quantities as the interacting system. To facilitate this need, the development of polaritonic exchange-correlation functionals is of intense research interest.^{45,75–77} A promising practical framework—the linear response theory of nonrelativistic QED—has also been developed,³¹ and it has been recently implemented using the Gaussian atomic basis.⁷⁸

In QEDFT, the spatial and photon wave functions are factorized, allowing the separation of the electronic and photonic components. One, then, has to solve coupled equations for the matter and photon parts. The dimensionality limits the product basis approaches to a few photon modes, while the QEDFT can be applied to hundreds of thousands of photon modes.³¹ More details and applications of the QEDFT method and its time-dependent version can be found in Refs. 25, 26, 28, 31, and 49.

In this paper, we present a QED-DFT [and Quantum-Electrodynamical Time-Dependent Density Functional Theory (QED-TDDFT)] approach, using a coupled electron-photon wave function similar to that shown in Eq. (1.1). The wave function will be defined on a tensor product (TP) of a spatial grid and Fock state representation. To distinguish this approach from the aforementioned QEDFT approach, we will call the present approach QED-DFT-TP and QED-TDDFT-TP. The QED-DFT-TP is a particular realization of the QEDFT theory using a different ansatz – a coupled electron-photon wave function. Unlike the Gaussian basis matrix formulation of the linear response QED-TDDFT in Ref. 78, the present approach uses explicit time propagation in solving the QED-TDDFT equations.

The tensor product form increases the dimensionality; however, it preserves the quantized photon states. In this way, we have direct access to non-classical observables of the photon field; e.g., the photon-number, the purity, and the Mandel Q number.⁷⁹ The coupled electron-photon wave function provides a more complex description of the light-matter interaction, by calculating the spatial wave function in each photon sector.

Each orbital of the molecule is coupled with different Fock basis states (photon states) describing the quantized light. The light-matter coupling part of the Hamiltonian will describe the interaction between the orbital components in different photons states. The Fock states are orthogonal, preserving and even increasing the sparsity of the real-space based DFT Hamiltonian. This sparsity allows the use of the efficient, iterative diagonalization approaches traditionally used in real-space DFT approaches.

As the coupling part and the product ansatz are simple, the present approach can be easily implemented in any real-space approaches. Plane-wave or orbital-based DFT methods can see similarly simple adaptation.

The approach will be tested using time-dependent and time-independent problems and our results will be compared to QED-SVM, QED-CC, and QEDFT calculations. One expects that the approach can be used anywhere where regular DFT and TDDFT have been useful, from bond length and density distribution

calculations, to descriptions of high harmonic generation and optical absorption.

II. FORMALISM

A. Hamiltonian

We assume that the system is nonrelativistic and the coupling to the light can be described by the dipole approximation. The Pauli–Fierz non-relativistic QED Hamiltonian provides a consistent quantum description at this level.^{26,30,43,51,67} The dipole approximation assumes that the spatial variation of the electric field is negligible across the size of the system – physically valid if the system size is much smaller than the wavelength of light. The PF Hamiltonian in the Coulomb gauge is $H = H_e + H_{ep}$, where H_e is the electronic Hamiltonian and

$$\begin{aligned} H_{ep} &= \sum_{\alpha=1}^{N_p} \frac{1}{2} \left[p_{\alpha}^2 + \omega_{\alpha}^2 \left(q_{\alpha} - \frac{\lambda_{\alpha}}{\omega_{\alpha}} \mathbf{D} \right)^2 \right], \\ &= \sum_{\alpha=1}^{N_p} \left[\omega_{\alpha} \left(\hat{a}_{\alpha}^+ \hat{a}_{\alpha} + \frac{1}{2} \right) - \omega_{\alpha} q_{\alpha} \lambda_{\alpha} \mathbf{D} + \frac{1}{2} (\lambda_{\alpha} \mathbf{D})^2 \right] \end{aligned} \quad (2.1)$$

(atomic units are used in this work). In Eq. (2.1), \mathbf{D} is the dipole operator, the photon fields are described by quantized oscillators, and $q_{\alpha} = \frac{1}{\sqrt{2\omega_{\alpha}}} (\hat{a}_{\alpha}^+ + \hat{a}_{\alpha})$ is the displacement field. Here \hat{a} and \hat{a}^+ are the lowering and raising operators of the quantized harmonic oscillator, respectively. This Hamiltonian describes N_p photon modes, with photon frequency ω_{α} and coupling λ_{α} . The coupling term is written as⁷³ $\lambda_{\alpha} = 1/\sqrt{\epsilon_0} \mathbf{u}_{\alpha}(\mathbf{r}_0)$, where $\mathbf{u}_{\alpha}(\mathbf{r})$ is the cavity mode function, and \mathbf{r}_0 is the center of the cavity where the molecule is placed. The first term in Eq. (2.1) is the Hamiltonian of the photon modes, the second term couples the photons to the dipole, and the last term is the dipole self-interaction (DSI)

$$H_d = \frac{1}{2} \sum_{\alpha=1}^{N_p} (\lambda_{\alpha} \mathbf{D})^2.$$

For the electronic Hamiltonian, we adopt the Kohn–Sham (KS) TDDFT⁸⁰ description

$$H_e = -\frac{\hbar^2}{2m} \nabla^2 + V_{KS}(\mathbf{r}), \quad (2.2)$$

with

$$V_{KS}(\mathbf{r}) = V_H[\rho](\mathbf{r}) + V_{XC}[\rho](\mathbf{r}) + V_{ion}(\mathbf{r}). \quad (2.3)$$

Here, ρ is the electron density, V_H is the Hartree potential, and V_{XC} is the exchange-correlation potential [Local density approximation (LDA) is used], and V_{ion} is the external potential due to the ions. The potential of the ions can be represented by employing the norm-conserving pseudopotentials of the form given by Troullier and Martins.⁸¹ We assume that the nuclei are fixed in their positions.

One should emphasize at this point, that the proper way of introducing the Hamiltonian would be to use mapping theorems

following the steps of Refs. 27, 73, and 75. See also Ref. 76 for recent developments. Our approach can be thought to be using the conventional velocity gauge TDDFT Hamiltonian as a starting point:

$$H_V = \frac{1}{2} \left(-i\hbar\nabla - \frac{e}{c}\mathbf{A} \right)^2 + V_{KS}(\mathbf{r}). \quad (2.4)$$

Then, we replace the classical vector potential with the quantized vector potential of the cavity

$$\hat{\mathbf{A}}(\mathbf{r}) = \sum_{\alpha} \left(\frac{\hbar}{2\epsilon_0\omega_{\alpha}} \right)^{1/2} [\hat{a}_{\alpha}\mathbf{u}_{\alpha}(\mathbf{r}) + \hat{a}_{\alpha}^{\dagger}\mathbf{u}_{\alpha}^{*}(\mathbf{r})]. \quad (2.5)$$

In the dipole approximation, placing the molecule in the middle of the cavity at \mathbf{r}_0 , one has

$$\hat{\mathbf{A}}(\mathbf{r}_0) = \sum_{\alpha} \lambda_{\alpha} (\hat{a}_{\alpha} + \hat{a}_{\alpha}^{\dagger}), \quad (2.6)$$

and

$$H_V = \frac{1}{2m} \left(-i\hbar\nabla - \frac{e}{c} \hat{\mathbf{A}}(\mathbf{r}_0) \right)^2 + V_{KS}(\mathbf{r}). \quad (2.7)$$

One can use a unitary transformation to transform the Hamiltonian into length gauge^{67,82}

$$H_L = U^{\dagger} H_V U, \quad (2.8)$$

with

$$U = \exp \left\{ \frac{ie}{\hbar c} \hat{\mathbf{A}}(\mathbf{r}_0) \cdot \mathbf{D} \right\}. \quad (2.9)$$

After a straightforward calculation,⁶⁷ one has

$$H_L = -\frac{\hbar^2}{2m} \nabla^2 + V_{KS}(\mathbf{r}) + \sum_{\alpha=1}^{N_p} \frac{1}{2} \left[p_{\alpha}^2 + \omega_{\alpha}^2 \left(q_{\alpha} - \frac{\lambda_{\alpha}}{\omega_{\alpha}} \mathbf{D} \right)^2 \right]. \quad (2.10)$$

Either H_V or H_L can be used in the calculations. The advantage of H_V is that one can use it with periodic boundary conditions. In either case, the Hamiltonian depends not only on the spatial coordinates, but also on the photon creation and annihilation operators, and one has to use a tensor product of the spatial and number state bases for the orbitals. We will use $H = H_L$ in this work.

B. Basis functions

The $\omega_{\alpha}q_{\alpha}\lambda_{\alpha}\mathbf{D}$ term couples the electronic and photonic degrees of freedom. The orbitals of the coupled electron and photon system at the KS level can be written as

$$\Phi_{mn} = \phi_{mn}(\mathbf{r})|n\rangle, \quad (m = 1, \dots, N_{occ}), \quad (n = 0, \dots, N_F), \quad (2.11)$$

where $|n\rangle$ is the Fock space basis for the photons, N_F is the dimension of the Fock space, and N_{occ} is the number of orbitals. In the

following, we assume that there is one dominant photon mode – $N_p = 1$ in Eq. (2.1) – with frequency ω . Extension to $N_p > 1$ is possible, but it quickly leads to prohibitively large basis dimensions. We use a real-space representation^{83–86} for the electronic part

$$\phi_{mn}(\mathbf{r}) = \phi_{mn}(x, y, z), \quad (2.12)$$

and the orbitals will be defined on a four dimensional (4D) product grid of the three dimensional real-space grid and the one dimensional Fock space. The 4D grid has $N_x \times N_y \times N_z \times (N_F + 1)$ grid points, where N_x, N_y, N_z are the grid points in real-space, and N_F is the size of the Fock basis. The orbitals are written as

$$\Phi_m(\mathbf{r}) = \begin{pmatrix} \Phi_{m0}(x_i, y_j, z_k) \\ \Phi_{m1}(x_i, y_j, z_k) \\ \vdots \\ \Phi_{mn}(x_i, y_j, z_k) \\ \vdots \end{pmatrix}. \quad (2.13)$$

Due to the orthogonality of the Fock basis states, we have

$$\langle \Phi_{mn} | \Phi_{m'n'} \rangle = \langle \phi_{mn} | \phi_{m'n'} \rangle \delta_{nn'}, \quad (2.14)$$

where the round bracket stands for the integration over the real and Fock space, and the angle bracket is the integration over the space part, with

$$\langle \phi_{mn} | \phi_{m'n'} \rangle = \sum_{ijk} \phi_{mn}(x_i, y_j, z_k) \phi_{m'n'}(x_i, y_j, z_k). \quad (2.15)$$

Using Gram–Schmidt orthogonalization, the real-space functions $\phi_{1n}, \dots, \phi_{N_{occ}n}$ are orthogonalized for each Fock state ($n = 0, \dots, N_F$). The new orthogonal set $\hat{\phi}_{1n}, \dots, \hat{\phi}_{N_{occ}n}$ is normalized

$$\sum_{n=0}^{N_F} |\hat{\phi}_{mn}|^2 = 1. \quad (2.16)$$

Now, one can define the electron density as

$$\rho(\mathbf{r}) = \sum_{m=1}^{N_{occ}} c_m \sum_{n=0}^{N_F} |\hat{\phi}_{mn}(\mathbf{r})|^2, \quad (2.17)$$

where c_m is the number of electrons on the m th orbital. One can also define the density belonging to a given Fock state as

$$p_n(\mathbf{r}) = \sum_{m=1}^{N_{occ}} c_m |\hat{\phi}_{mn}(\mathbf{r})|^2, \quad (2.18)$$

and the photon occupation probability in the Fock space

$$P_n = \frac{1}{N} \int p_n(\mathbf{r}) d\mathbf{r}, \quad (2.19)$$

where N is the number of electrons.

The orbitals will be calculated by iterative minimization – conjugate gradient in the present case – in the same way as in the conventional real-space approaches. For this, we need to calculate the action of the Hamiltonian on the wave function. Noting that

$$\omega \left(\hat{a}^+ \hat{a} + \frac{1}{2} \right) |n\rangle = \left(n + \frac{1}{2} \right) \omega |n\rangle, \quad (2.20)$$

and

$$\begin{aligned} q|n\rangle &= \frac{1}{\sqrt{2\omega}} (\hat{a} + \hat{a}^+) |n\rangle, \\ &= \frac{1}{\sqrt{2\omega}} \left(|\sqrt{n}|n-1\rangle + \sqrt{n+1}|n+1\rangle \right), \end{aligned} \quad (2.21)$$

one has

$$\begin{aligned} H\Phi_{mn}(\mathbf{r}) &= -\frac{1}{2} \nabla^2 \Phi_{mn}(\mathbf{r}) + \left(V_{KS}(\mathbf{r}) + \mu(\lambda\mathbf{r}) + \omega \left(n + \frac{1}{2} \right) \right) \Phi_{mn}(\mathbf{r}) \\ &\quad - \sqrt{\frac{\omega}{2}} (\lambda\mathbf{r}) \left(\sqrt{n}\Phi_{mn-1}(\mathbf{r}) + \sqrt{n+1}\Phi_{mn+1}(\mathbf{r}) \right), \end{aligned} \quad (2.22)$$

where

$$\mu = \int \lambda \mathbf{r} \rho(\mathbf{r}) d\mathbf{r}. \quad (2.23)$$

In the first part of this equation, the Hamiltonian acts on ϕ_{mn} in each Fock space in the same way as in conventional real-space approaches. The kinetic energy operator is represented by nine-point finite differencing, and the non-local part of the pseudopotential is calculated by a summation of the pseudopotential core radius around the atomic position, leading to a very sparse Hamiltonian matrix. In the second part of the equation, the photon spaces n and $n \pm 1$ are connected, and the coupling Hamiltonian matrix is diagonal. This large sparse system is ideal for iterative approaches.

C. Ground state calculation

The ground state calculation is similar to the conventional DFT calculations:

- Initialization of the orbitals. $\phi_{mn}^{(0)}$ are approximated, e.g., by atomic orbitals. The components belonging to the lowest ($n = 0, 1$) Fock spaces are expected to be dominant; so, a weight factor is used to enhance those components, $\phi_{mn}^{(0)} \rightarrow w_n \phi_{mn}^{(0)}$. Orthogonalize the orbitals to generate the starting wave function

$$\Phi_m^{(0)}(\mathbf{r}) = \begin{pmatrix} \hat{\Phi}_{m0}^{(0)}(\mathbf{r}) \\ \hat{\Phi}_{m1}^{(0)}(\mathbf{r}) \\ \vdots \\ \hat{\Phi}_{mn}^{(0)}(\mathbf{r}) \\ \vdots \end{pmatrix}, \quad (2.24)$$

where $\hat{\Phi}_{mn}^{(0)}(\mathbf{r}) = \hat{\phi}_{mn}^{(0)}(\mathbf{r})|n\rangle$.

- Iterative minimization step. Use

$$\Phi_m^{(k+1)}(\mathbf{r}) = \sum_j a_j H^j \hat{\Phi}_m^{(k)}(\mathbf{r}), \quad (2.25)$$

where the a_j coefficients define the iterative procedure, e.g., steepest descent, conjugate gradient, and imaginary time-propagation. Equation (2.22) is used to calculate $H\hat{\Phi}_{mn}^{(k)}$.

- Calculate $\hat{\Phi}_m^{(k+1)}(\mathbf{r})$ by Gram–Schmidt orthogonalization $\Phi_m^{(k+1)}(\mathbf{r})$.
- Calculate ρ and update V_{KS} .
- $k = k + 1$, go to step 2 until convergence is reached.

D. Time propagation

The ground state orbitals will be used to initialize the time propagation

$$\hat{\Phi}_m(\mathbf{r}, t = 0) = \hat{\Phi}_m(\mathbf{r}). \quad (2.26)$$

Any time propagation method typically used for TDDFT can be used here, and in this work, we use the Taylor time propagation⁸⁴

$$\hat{\Phi}_m(\mathbf{r}, t + \Delta t) = e^{-iH\Delta t} \hat{\Phi}_m(\mathbf{r}, t) = \sum_{j=0}^4 \frac{(-i\Delta t)^j}{j!} H^j \hat{\Phi}_m(\mathbf{r}, t), \quad (2.27)$$

where Δt is chosen to be sufficiently small to conserve the norm of the orbitals during propagation.

III. APPLICATIONS

Atomic units are used in the calculations, and we drop the “a.u.” notation after every number. The coupling will be defined as $\lambda = \lambda \mathbf{u}$, where \mathbf{u} is a unit vector, e.g., (1,0,0). λ can be related to the effective cavity volume $\lambda = 1/\sqrt{\epsilon_0 V_{eff}}$ (ϵ_0 is the permittivity of vacuum).⁸⁷ Sub nm³ volumes have been reached in picocavities^{88,89} corresponding to $\lambda < 0.05$, which will be the highest value that we consider in this work, except, for example, for benzene, in which we calculate the wave function in higher photon spaces. The convergence of the grid calculations is illustrated in Sec. III E.

A. Hydrogen molecule

In the first example, we calculate the energy of a hydrogen molecule in a cavity with fixed nuclei. Two-photon spaces, $|0\rangle$ and $|1\rangle$, are used. Higher photon spaces have negligible contribution for this coupling strength region. The results are compared to an SVM and a QED-CC calculation. As mentioned in the introduction, both, the SVM and the QED-CC, are very accurate wave function based approaches and are in complete agreement with each other in these calculations. Figure 1 shows the total energy as a function of bond length (denoted as d) for $\lambda = 0.05$ [$\lambda = (\lambda, 0, 0)$] and $\omega = 0.081$. The molecular bond lay parallel to the photon polarization vector. The parameters are chosen to make a comparison to the QED-CC calculations of Ref. 90. The calculated QED-DFT-TP energy is shifted with respect to QED-CC and SVM energies, due to the LDA and pseudopotential approximations, but the overall trend is

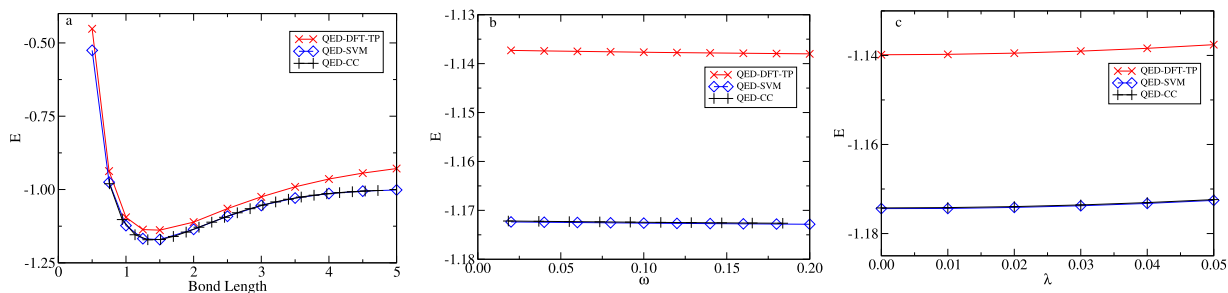


FIG. 1. Comparison of the results of the QED-DFT-TP, QED-CC, and QED-SVM calculations for energy dependence on bond length (a), ω (b), and λ (c). The QED-CC results are from the calculation of Ref. 90 using the cc-pVQZ basis. $\omega = 0.08$ is used for (a) and (c), $\lambda = 0.05$ is used for (a) and (b). $N_x = N_y = N_z = 81$ and $h = 0.5$ grid spacing used in the calculations.

similar. The only noticeable difference is in the $2 \leq d$ region, where the QED-DFT-TP curve has a larger slope. This is mainly due to the LDA approximation which performs well near the equilibrium separation, but is inaccurate when the bond is stretched, as discussed, e.g., in Refs. 91 and 92.

At this coupling strength, the effect of the coupling on the ground state is mainly an energy shift. It is more interesting to study the ω and λ dependence for a given bond length. This is shown in Figs. 1(b) and 1(c). The SVM and QED-CC results are in excellent agreement, and the QED-DFT-TP results show similar behavior, except for the energy shift.

Figure 2 compares the photon occupation number P_0 as a function of bond length λ and ω . $N_F = 1$ is used; so, $P_0 + P_1 = 1$, and only P_0 is shown in the figures. In the case of bond length, SVM and QED-DFT agree well up to $d = 1.7$. For larger distances, the two probabilities are different. As Fig. 1(a) shows, the energy of the H₂ molecule calculated by DFT is not accurate for large bond length, and the inaccuracy also appears in the photon occupation probability. In future calculations, it will be important to go beyond LDA and implement better exchange correlation functionals, to investigate whether they improve the photon occupation at larger bond length in the same way that they improve the energy.⁹² The SVM and QED-DFT-TP description of the λ and ω dependence agrees well.

B. The LiH and the HF molecules

Figures 3(a) and 3(b) show the λ and ω dependence of the energy of the LiH molecule. The ω dependence values calculated

by QED-SVM and QED-DFT-TP are very similar. Due to the pseudopotential approach, the total energies calculated by QED-DFT-TP and QED-SVM are different, and the QED-SVM energies are shifted up by a constant, to fit them in the same figure. We chose a larger ω ($\omega = 0.5$) for the calculation of the λ dependence to show the importance of the coupling of the $|0\rangle$ and $|1\rangle$ photon spaces. Figure 3(b) shows that the energy in the $|0\rangle + |1\rangle$ case is significantly lower than that in the $|0\rangle$ case for higher λ values (in the $|0\rangle$ space, only the dipole self-interaction is added to the Hamiltonian). The λ dependence values calculated by QED-SVM and the QED-DFT-TP are in good agreement.

Figures 3(c) and 3(d) show the λ and ω dependence for an HF molecule. The ω dependence values are very similar in both the QED-DFT-TP and QED-CC cases. The energy shift is due to the pseudopotential treatment of the core electrons in the QED-DFT-TP case. In this case, the weight of the $|0\rangle$ space is 95%, and the weight of the $|1\rangle$ space is 5% for the largest λ ; so, in the overall, the $|0\rangle$ space dominates, but the $|1\rangle$ space also contributes to the energy, as Fig. 3(d) shows.

The λ dependence only agrees in the tendency that by increasing λ the energy is increased, but the λ dependence is much larger in the QED-DFT-TP case.

C. Na₂ cluster

The next example is a Na₂ cluster, with a bond length $d = 5.8$. After the ground state calculation, the initial wave function is excited with a delta kick (see Appendix D for details) and then time

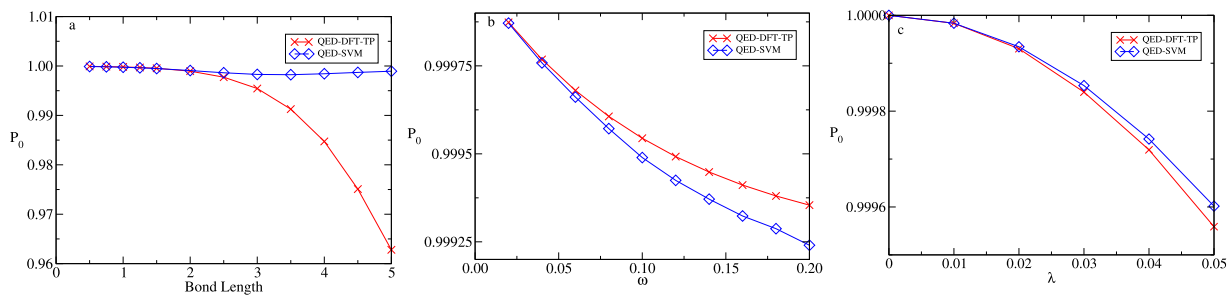


FIG. 2. Photon occupation number as a function of bond length (a), ω (b), and λ (c). $\omega = 0.08$ is used for (a) and (c), and $\lambda = 0.05$ is used for (a) and (b). $N_x = N_y = N_z = 81$ and $h = 0.5$ are used in the calculations.

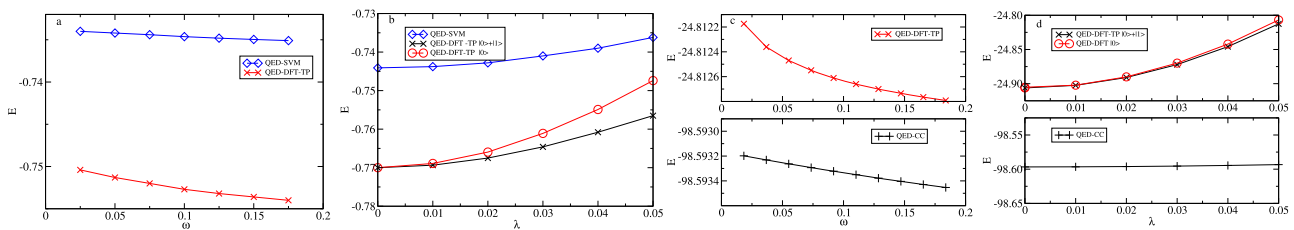


FIG. 3. Dependence of the energy of LiH on ω (a) and λ (b). Dependence of the energy of HF on ω (c) and λ (d). The Li-H distance is 3.015, and the H-F distance is 1.7229, $\lambda = 0.05$ was used to calculate the ω dependence for both molecules. For LiH $\omega = 0.5$ and for HF $\omega = 0.0813$, which were used to calculate the λ dependence. $N_x = N_y = N_z = 51$ grid points were used, with $h = 0.5$ grid spacing. The QED-CC results are from.³⁰ In the case of the LiH molecule the QED-SVM results are shifted up by 7.3.

propagated. We have also used the QEDFT approach (see Appendix B for details) to study the properties of Na_2 , to compare them to the QED-TDDFT-TP results. The time dependence of the dipole moment $D_x(t)$ is shown in Fig. 4(a). The dipole moments calculated by the two approaches show similarity, but not the same, because these quantities are calculated in different ways: one is solving Eq. (B1), while the other is using Eq. (2.22), in the coupled orbital and photon spaces.

What we are really interested in is the excitation spectra shown in Fig. 4(b). The single peak of the Na_2 spectrum when no cavity is present splits into two polariton peaks in the cavity in both QEDFT and the present calculation. The QEDFT predicts a somewhat bigger splitting, but both approaches show a larger upper polariton peak. The position of the di-sodium peak, while not in a cavity, seems to be at the position of the lower polariton peak of the present calculation. This is just a coincidence: the position of the single peak shifts to higher energies with non-zero λ , and the present calculation also predicts upper and lower polaritons with respect to the single peak. We will show this next.

Figure 4(c) shows the evolution of the Rabi splitting as a function of λ . Using the $|0\rangle$ space only, the dipole self-interaction changes the energy of the system and changes the position of the peak in the absorption cross section [Fig. 4(d)] compared to the “no cavity” case (no dipole self-interaction). By coupling the $|0\rangle$ and $|1\rangle$ photon spaces, the Rabi splitting appears in the form of two peaks:

one above and one below the single peak of the $|0\rangle$ photon space case. By increasing λ , the splitting is increasing, as expected. The figure also shows the contribution from the $|0\rangle$ component in the $|0\rangle + |1\rangle$ coupled case. For small λ , the $|0\rangle$ component is dominant (but there is no splitting without the coupling), but for larger λ [see Fig. 4(c) for $\lambda = 0.05$], the $|1\rangle$ space significantly contributes; in this case to the lower peak. Note that the width of the peaks is related to the length of the simulation time. The present model excludes physical mechanisms of line broadening. More time steps at a fixed temporal resolution result in narrower, Dirac-delta-like peaks.

D. Benzene and *p*-nitroaniline molecules

In this section, we show how the electron density changes in different photon spaces in cavities.¹⁶ The first example is a benzene molecule (see Fig. 5). In this case, we try a larger λ , to couple higher photon spaces in the wave function. The $|0\rangle$, $|1\rangle$, and $|2\rangle$ spaces are coupled, and the weights of these components are 0.94, 0.056, and 0.004, respectively. The electron density of benzene in the $|0\rangle$ photon space [Fig. 5(a)] is very similar to the ground state electron density. The density in the $|1\rangle$ photon space [Fig. 5(b)] is somewhat more compact than that in $|0\rangle$, and a density hole appears in the middle of the ring. The $|2\rangle$ density [Fig. 5(c)] is split perpendicular to the polarization vector $\lambda = (\lambda, \lambda, 0)$. This split is the consequence of the

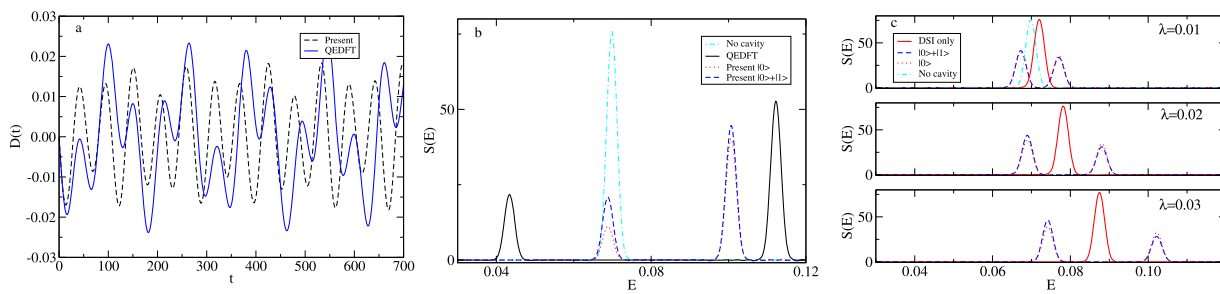


FIG. 4. QED-TDDFT-TP calculation for the Na_2 dimer. (a) Time dependence of the dipole moment. (b) Rabi splitting calculated by the QEDFT and by the present approach. $|0\rangle$ is the contribution to the absorption cross section from the 0 photon space in a calculation using the $|0\rangle + |1\rangle$ space, where $|0\rangle + |1\rangle$ is the total absorption cross section. $\lambda = (\lambda, 0, 0)$, $\lambda = 0.05$. (c) Dependence of the Rabi splitting on λ . DSI is the dipole self-interaction contribution. In this case, the molecule is in a cavity, but coupled only to the $|0\rangle$ photon space. The Na_2 dimer is oriented along the x direction, and the two atoms are $d = 5.8$ distance apart. $N_x = N_y = N_z = 51$, $h = 0.5$, $dt = 0.07$, $N_t = 10\,000$, and $d = 5.8$. $\omega = 0.07$ is used in the calculations.; $N_t = 30\,000$.

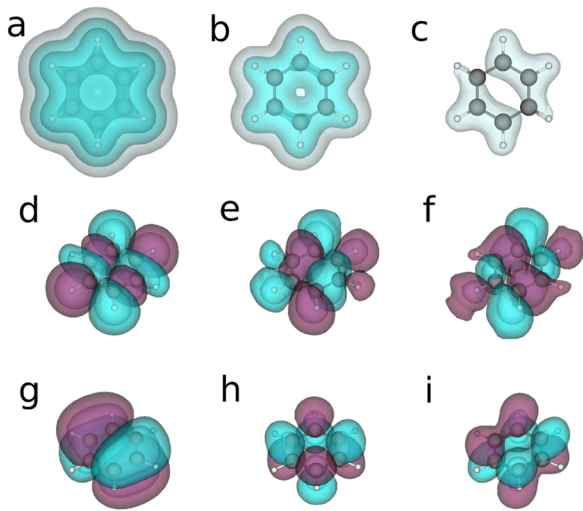


FIG. 5. Electron density isosurfaces of benzene in the (a) $|0\rangle$, (b) $|1\rangle$, and (c) $|2\rangle$ photon spaces. The three shades of the isosurfaces have values of 0.01, 0.001, and 0.0001, respectively. HOMO-2 orbital isosurfaces of benzene in the (d) $|0\rangle$, (e) $|1\rangle$, and (f) $|2\rangle$ photon spaces. HOMO orbital isosurfaces of benzene in the (g) $|0\rangle$, (h) $|1\rangle$, and (i) $|2\rangle$ photon spaces. $N_x = N_y = N_z = 51$ grid points are used with $h = 0.5$ grid spacing, $\lambda = (0.1, 0.1, 0)$ and $\omega = 0.5$. The darker (magenta) color shows the positive and the lighter (cyan) color shows the negative values. The two shades of the isosurfaces have values of 0.0005 and 0.0002, respectively.

symmetry breaking introduced by the λ dependent parts of the H_{ep} term in Eq. (2.1).

Figures 5(d)–5(i) show the HOMO-2 and the HOMO orbitals. The orbitals in the $|0\rangle$ photon space remain very similar to the ground state orbitals (the slight modification due to the dipole self-interaction is not visible in the figures). The $|1\rangle$ and the $|2\rangle$ components of the HOMO-2 and HOMO orbitals [Figs. 5(e), 5(f), 5(g), and 5(i)] are significantly different from the $|0\rangle$ component. In the case of HOMO-2, only the charge distribution changes, and the shapes of the orbital components are similar, but in the case of the HOMO, the lobes are also different. Other orbitals (not shown) have similar shape changes.

The next example is a *p*-nitroaniline molecule, which was studied by QED-CC in Ref. 71, and we have adopted the parameters from that work. This is an example of a molecule with a low-lying charge transfer excitation. To measure the charge transfer, one can define⁷¹

$$\Delta q(x) = \int_{-\infty}^x dx \int_{-\infty}^{\infty} dy \int_{-\infty}^{\infty} dz \Delta \rho(x, y, z), \quad (3.1)$$

$$\Delta \rho(x, y, z) = \rho^{cavity}(x, y, z) - \rho^{nocavity}(x, y, z). \quad (3.2)$$

$\Delta q(x)$ measures the amount of charge moved in the x direction – the principle axis of the molecule. The density difference induced in the molecule by the cavity is shown in Fig. 6. The charge redistribution is similar to what is shown in Ref. 71. Electrons transfer from the nitro (NO_2) side to the aniline (NH_2) side. The $\Delta q(x)$ function shown in Fig. 6 is also very similar to the QED-CC calculation in Ref. 71.

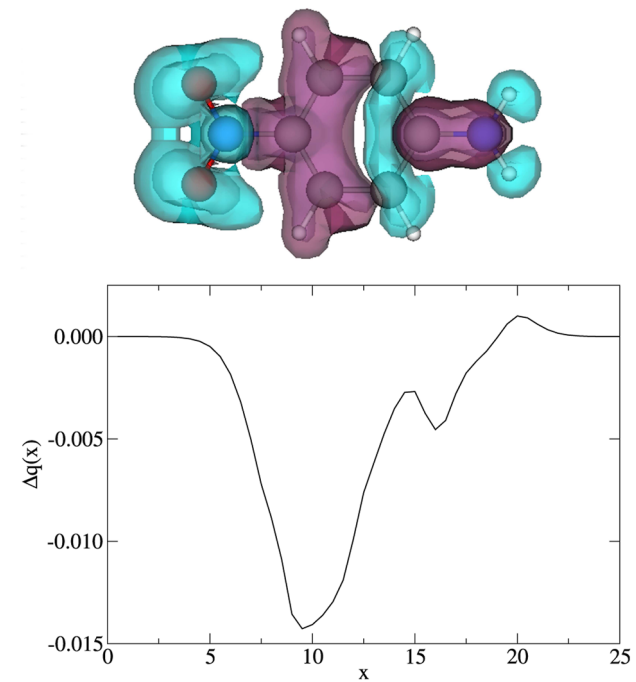


FIG. 6. (top) The cavity induced density difference between of a *p*-nitroaniline molecule in cavity shown as isosurfaces. The two shades of the isosurfaces have values of 0.0005 and 0.0002, respectively. (bottom) Charge distribution of a *p*-nitroaniline molecule in cavity. $\lambda = (0.05, 0, 0)$ and $\omega = 0.178$ values were used in the calculation. $N_x = N_y = N_z = 55$ grid points were used with $h = 0.5$ grid spacing. The lighter (cyan) and darker (magenta) regions represent charge depletions and accumulations, respectively.

We have also calculated the optical absorption spectrum of the benzene molecule in a cavity by time propagating the dipole moment after an initial delta kick perturbation. The Rabi splittings for benzene is shown in Fig. 7. The calculated splittings are 0.22 (0.33), 0.63 (0.69), 0.81 (1.02), 1.03 (1.35) for $\lambda = 0.01, 0.02, 0.03, 0.04$, respectively. The numbers in the parenthesis are from Ref. 31. Just as in the case of the Na_2 cluster, our QED-TDDFT-TP approach gives somewhat smaller Rabi splitting than the QEDFT approach, but the overall trend—a direct proportionality between the splitting and λ —is the same.

E. High harmonic generation

As a final example, we present the high harmonic spectrum of the HF molecule with and without a cavity. The molecule is excited with a continuous laser pulse

$$E(\mathbf{r}, t) = (E_x, 0, 0) \sin(\pi t/(6T_L))^2 \sin(\omega_L t), \quad (3.3)$$

and after 30 laser cycles, the high harmonic spectrum is calculated using the dipole acceleration

$$I(\omega) = \left| \int_0^T \frac{\partial^2 \mathbf{D}(t)}{\partial t^2} e^{-i\omega t} dt \right|^2. \quad (3.4)$$

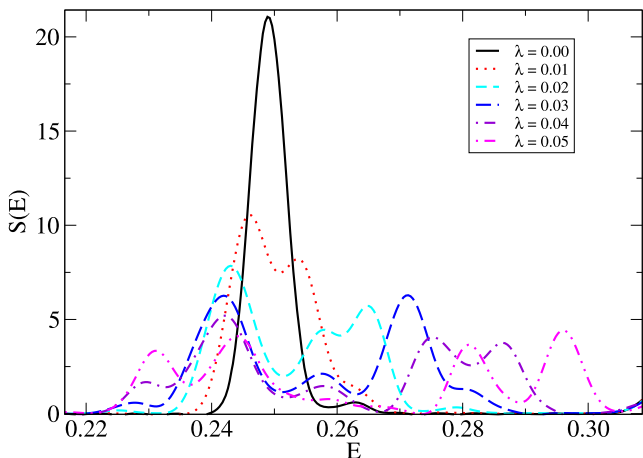


FIG. 7. Rabi splitting for benzene for different λ values. $N_x = N_y = N_z = 55$ grid points is used with $h = 0.5$ grid spacing. The time step is 0.05 and the total propagation time is 1000. $\lambda = (0, \lambda, 0)$ and $\omega = 0.25$ was used in the calculations.

Figure 8 shows the calculated high harmonics. We are mostly interested in the first few harmonics and use a relatively small computational box to speed up the calculations. To resolve more harmonics, one needs a larger box, which increases the computational cost.

If no cavity is present, the harmonic spectrum of the HF molecule oriented in the direction of the polarization of the laser consists of peaks at $n\omega_L$ (see Fig. 8 for the $\omega = 0$ case). Since the HF

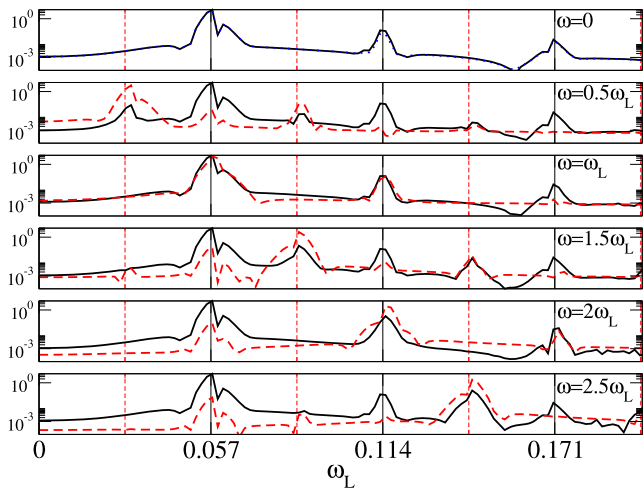


FIG. 8. High harmonics spectrum of the HF molecule (black lines). The red dashed lines show the contribution from the $|1\rangle$ photon space. The blue dotted line shows the high harmonics of the HF molecule without the cavity. The solid vertical lines show the position of $n\omega_L$, the dashed vertical lines are at $(n + 1/2)\omega_L$ (where n is an integer). The axis of the molecule is in the x direction, the H-F distance is 1.7229, $N_x = N_y = N_z = 51$, $h = 0.5$, $\lambda = (0.05, 0, 0)$, $\Delta t = 0.05$, and $\omega = 0.081$ were used. The laser is polarized in the x direction, and the laser parameters are $\omega_L = 0.057$ (800 nm wavelength), $T_L = 2/\omega_L$, and $E_x = 0.005$.

does not have inversion symmetry, both the even and odd harmonics are present. With placing the molecule in a cavity using the $|0\rangle$ photon space only, the high harmonic spectrum of the HF molecule does not change (the solid black and dotted blue lines are barely distinguishable in Fig. 8).

Using the $|0\rangle + |1\rangle$ photon spaces, new peaks appear in the harmonic spectrum at $\omega + n\omega_L$ positions. For example, if $\omega = 0.5\omega_L$, then the new peaks are at $0.5\omega_L + n\omega_L$ (Fig. 8). These peaks have significant intensity, and the peaks are present at weaker and stronger couplings as well. If $\omega = n\omega_L$, the new (cavity induced) peaks coincide with peaks of the laser, and the spectrum remains very similar to the harmonic spectrum without a cavity. Figure 8 also shows the contribution from the $|1\rangle$ photons spaces. The dipole moment is the sum of the components from the $|0\rangle$ and $|1\rangle$ photon spaces, and the harmonic spectrum is a result of an interference of these terms. Figure 8 shows that in the case of $\omega = (k + 1/2)\omega_L$ ($k = 0, 1, 2, \dots$), the $|1\rangle$ component has pronounced peaks at $\omega, \omega + \omega_L$ and $\omega + 2\omega_L$. The $|1\rangle$ photon space not only induces new peaks, but significantly contributes to their intensity as well.

IV. SUMMARY

We have developed and implemented a QED-TDDFT-TP approach that uses a direct product of a Fock space for light and a real-space grid for electrons. We have tested the approach by comparing it to accurate QED-SVM and QED-CC calculations, and the results are very promising. The coupling strength and light frequency dependence of energies calculated by the present approach are very similar to the QED-SVM and QED-CC results.

One of the main advantages of the approach is that, it preserves the quantized photon spaces, giving direct access to non-classical photon observables. A further important advantage is that, as the electron and the photon coordinates are separated, one can assess the contribution to physical quantities from different photon spaces.

The light-matter coupling strongly modifies the molecular orbitals, and the orbitals have very different shapes in different photon spaces. This also leads to charge transfer and redistribution, and our results are similar to the QED-CC calculation.⁷¹

We have also studied the Rabi splitting in molecules in optical cavities, and the results show that the splitting is caused by the presence of light states: there is no splitting without the presence of $|0\rangle$ and $|1\rangle$ photon spaces.

The approach can also be used to study high harmonic generation in strongly coupled light-matter coupled systems. There are several recent experimental and theoretical works studying the influence of polaritons on non-linear optical processes.^{93–97} We plan to extend the present study, to describe the high harmonic generation for more complex molecules. We also plan to calculate the non-linear susceptibilities of molecules in cavities, combining the present approach with the method described in Ref. 98.

The tensor product of the real-space and Fock-space increases with the number of Fock spaces. For experimentally realizable strong coupling one needs $N_F = 2$ or $N_F = 3$ Fock space dimensions for a single photon frequency. This increases the cost of the calculation in time and memory requirements by a factor of N_F . If more than one photon frequency is necessary, then the calculation cost increases by $N_F^{N_p}$, where N_p is the number of relevant photon modes. For larger

N_p , this will be prohibitively expensive, and one needs alternatives, such as the QEDFT approach, which can handle any number of photons.

The increased dimensionality is not the only complicating factor. The Hamiltonian (2.22) (except from a trivial $n\omega$ shift) acts the same way on every real-space component $\phi_{mn}(\mathbf{r}, t)$ for a given photon number. If there would be no coupling in the Hamiltonian, then one would have the same set of $\phi_{mn}(\mathbf{r}, t)$, ($m = 1, \dots, N_{occ}$) orbitals in each $|n\rangle$ photon space. In the self-consistent iterative diagonalization of the non-linear Hamiltonian, one has to carefully mix the density, so that the photon components are gradually optimized. The process is very sensitive to the coupling (the off-diagonal part of the Hamiltonian), because the coupling makes the orbitals different in different photon spaces. Sudden changes in the density lead to slow, damped oscillatory convergence. Future work is necessary for optimizing the self-consistent solution for this tensor product approach, in order to have efficient calculations.

The development of accurate exchange-correlation functionals is also important for future calculations. In the present work, we have compared our calculations with QED-SVM and QED-CC results, and these approaches may help in developing appropriate functionals for QED-TDDFT-TP.

ACKNOWLEDGMENTS

This work has been supported by the National Science Foundation (NSF) under Grant No. IRES 1826917. We thank Angel Rubio for the useful discussions and clarifications.

AUTHOR DECLARATIONS

Conflict of Interest

The authors have no conflicts to disclose.

Author Contributions

J.M., A.A., and D.P. equally contributed to this work.

Justin Malave: Formal analysis (equal); Investigation (equal); Visualization (equal); Writing – review & editing (supporting). **Alexander Ahrens:** Investigation (equal); Visualization (equal). **Daniel Pitagora:** Investigation (equal); Visualization (equal). **Cody Covington:** Investigation (equal); Supervision (equal); Visualization (equal); Writing – review & editing (supporting). **Kálmán Varga:** Funding acquisition (lead); Investigation (equal); Supervision (lead); Writing – original draft (lead).

DATA AVAILABILITY

The data that support the findings of this study are available from the corresponding author upon reasonable request.

APPENDIX A: PHOTON SPACE

In this Appendix, we give a brief overview of the properties of the Fock space and occupation number bases. The photon Hamiltonian [from Eq. (2.1)] is

$$H_p = \sum_{\alpha=1}^{N_p} \frac{1}{2} (p_{\alpha}^2 + \omega_{\alpha}^2 q_{\alpha}^2) = \sum_{\alpha=1}^{N_p} \omega_{\alpha} \left(\hat{a}_{\alpha}^{\dagger} \hat{a}_{\alpha} + \frac{1}{2} \right), \quad (\text{A1})$$

where

$$q_{\alpha} = \frac{1}{\sqrt{2\omega_{\alpha}}} (\hat{a}_{\alpha} + \hat{a}_{\alpha}^{\dagger}) \quad p_{\alpha} = \frac{1}{i\sqrt{2\omega_{\alpha}}} (\hat{a}_{\alpha} - \hat{a}_{\alpha}^{\dagger}). \quad (\text{A2})$$

Denoting the vacuum state as $|0\rangle$, any eigenstate of $\hat{a}_{\alpha}^{\dagger} \hat{a}_{\alpha}$ can be calculated by multiple applications of the creation operators

$$|n_{\alpha}\rangle = \frac{1}{\sqrt{n!}} (\hat{a}_{\alpha}^{\dagger})^n |0\rangle. \quad (\text{A3})$$

This is called the occupation number representation; n_{α} defines the excited state of the ω_{α} photon mode. The bosonic operators satisfy the commutation relations

$$[\hat{a}_{\alpha}, \hat{a}_{\alpha'}] = [\hat{a}_{\alpha}^{\dagger}, \hat{a}_{\alpha'}^{\dagger}] = 0, \quad [\hat{a}_{\alpha}, \hat{a}_{\alpha'}^{\dagger}] = \delta_{\alpha, \alpha'} \hat{1}, \quad (\text{A4})$$

where $[a, b] = ab - ba$.

Now one can define an occupation number basis

$$\chi_{\vec{n}} = |n_1, n_2, \dots, N_p\rangle = \frac{1}{\sqrt{n_1! \dots n_{N_p}!}} (\hat{a}_1^{\dagger})^{n_1} \dots (\hat{a}_{N_p}^{\dagger})^{n_{N_p}} |0\rangle, \quad (\text{A5})$$

where $n = n_1 + \dots + N_p$. In this abstract space representation, the symmetry requirement for bosons is satisfied by allowing mode i to be occupied by n_i photons. For the product state in Eq. (A5), the restriction to the symmetric subspace is tacitly assumed—that is, one has to symmetrize the states for identical harmonic oscillators.

APPENDIX B: QEDFT

In the approach of Refs. 25, 26, 28, 31, and 49, two coupled equations are solved:

$$i\hbar \frac{\partial}{\partial t} \varphi_i(\mathbf{r}, t) = \left(-\frac{1}{2} \nabla^2 + V_{KS}(\mathbf{r}, t) + V_P(\mathbf{r}, q, t) \right) \varphi_i(\mathbf{r}, t), \quad (\text{B1})$$

$$\left(\frac{\partial^2}{\partial t^2} + \omega_{\alpha}^2 \right) q_{\alpha}(t) = -\frac{j_{\alpha}(t)}{\omega_{\alpha}} + \omega_{\alpha} \boldsymbol{\lambda}_{\alpha} \cdot \mathbf{R}(t), \quad (\text{B2})$$

where $\mathbf{R}(t) = \int d\mathbf{r} \mathbf{r} \rho(\mathbf{r}, t)$. The photon exchange potential is

$$V_P(\mathbf{r}, q, t) = \sum_{\alpha=1}^M \left(\int d\mathbf{r}' \boldsymbol{\lambda}_{\alpha} \cdot \mathbf{r}' \rho(\mathbf{r}', t) - \omega_{\alpha} q_{\alpha}(t) \right) \boldsymbol{\lambda}_{\alpha} \mathbf{r}. \quad (\text{B3})$$

The photon is propagated as

$$\left(\frac{\partial^2}{\partial t^2} + \omega_{\alpha}^2 \right) q_{\alpha}(t) = \omega_{\alpha} \boldsymbol{\lambda}_{\alpha} \mathbf{R}(t). \quad (\text{B4})$$

APPENDIX C: STOCHASTIC VARIATIONAL APPROACH

In this case, the full Coulombic Hamiltonian is used; the Hamiltonian of an N electron system interacting with a Coulomb interaction and confined in an external potential V_c is

$$H_e = -\sum_{i=1}^N \frac{\nabla_i^2}{2m_i} + \sum_{i < j}^N \frac{q_i q_j}{|\mathbf{r}_i - \mathbf{r}_j|} + \sum_{i=1}^N V_c(\mathbf{r}_i), \quad (\text{C1})$$

where \mathbf{r}_i , q_i , and m_i are the coordinate, charge, and mass of the i th particle ($m_i = 1$ for electrons in atomic units), respectively.

Introducing the shorthand notations $\vec{r} = (\mathbf{r}_1, \dots, \mathbf{r}_N)$, the variational trial wave function is written as a linear combination of products of spatial and photon space basis functions

$$\Psi(\vec{r}) = \sum_n \sum_{k=1}^{K_n} c_k^n \psi_k^n(\vec{r}) |n\rangle. \quad (\text{C2})$$

The spatial part of the wave function is expanded into ECGs for each photon state $|n\rangle$ as

$$\psi_k^n(\vec{r}) = \mathcal{A} \left\{ e^{-\frac{1}{2} \sum_{i < j}^N \alpha_{ij}^k (\mathbf{r}_i - \mathbf{r}_j)^2 - \frac{1}{2} \sum_{i=1}^N \beta_i^k (\mathbf{r}_i - \mathbf{s}_i^k)^2} \chi_S \right\}, \quad (\text{C3})$$

where \mathcal{A} is an antisymmetrizer, χ_S is the N electron spin function (coupling the spin to S), and α_{ij}^k , β_i^k and \mathbf{s}_i^k are non-linear parameters. The basis functions are optimized as described in Ref. 68.

APPENDIX D: ABSORPTION CROSS SECTION

The polarizability tensor $\boldsymbol{\alpha}(\omega)$ can be calculated by time propagation of the electron orbital states. The initial state is first perturbed by a delta kick potential

$$V_{ext} = -e\mathbf{r} \cdot \mathbf{k}_i \delta(t_0), \quad (\text{D1})$$

where \mathbf{k}_i is the electric field in the i direction ($i = x, y, z$). The magnitude of the electric field should be sufficiently small to initiate a linear response.

The polarizability tensor in frequency space is defined as the Fourier transform of the time-dependent dipole moment

$$\alpha_{ij}(\omega) = \frac{1}{k_i} \int_0^\infty dt [D_j(t) - D_j(t_0)] e^{-i\omega t}. \quad (\text{D2})$$

The time-dependent dipole moments can be calculated from the time-dependent electronic density $[\rho(\mathbf{r}, t)]$:

$$\mathbf{D}(t) = \int \mathbf{r} \cdot \rho(\mathbf{r}, t) d\mathbf{r}. \quad (\text{D3})$$

The imaginary part of the dynamic polarizability tensor can be related to the oscillator strength of each transition⁹⁹

$$\begin{aligned} \frac{1}{3} \text{Tr}(\Im m \boldsymbol{\alpha}(\omega)) &= \frac{\pi}{3} \sum_{n=1}^{\infty} \sum_{v=1}^3 |\langle \Psi_0 | \hat{r}_v | \Psi_n \rangle|^2 \delta(\omega - \Omega_n), \\ &= \sum_{n=1}^{\infty} \frac{\pi}{2\Omega_n} f_n \delta(\omega - \Omega_n), \end{aligned} \quad (\text{D4})$$

where the $|\Psi_n\rangle$ is the wave function of the n -th excited state, Ω_n is the corresponding excitation energy, and f_n is the oscillator strength belonging to the transition probability for the excitation. The dynamic polarization tensor $[\boldsymbol{\alpha}(\omega)]$ and the transition dipole moment are now connected as ($\mathbf{D}_{n0} = \langle \Psi_0 | \hat{r} | \Psi_n \rangle$).

From the imaginary part of the dynamic polarizability tensor, one can extract the photo-absorption cross-section

$$\sigma(\omega) = \frac{4\pi\omega}{3c} \text{Tr}[\Im m(\boldsymbol{\alpha}(\omega))] = \frac{2\pi^2}{c} S(\omega), \quad (\text{D5})$$

where c is the speed of light and $S(\omega) = \sum_{n=1}^{\infty} f_n \delta(\omega - \Omega_n)$ is the dipole spectral function.

A damping function is added to the Fourier transform of the photo-absorption spectrum for finite propagation times. The damping function introduces an artificial decay of the excited population to smooth spectrum. We use a Gaussian damping function ($e^{-\eta^2 t^2}$), and the parameter η is chosen to make the damping very small at the end of propagation.

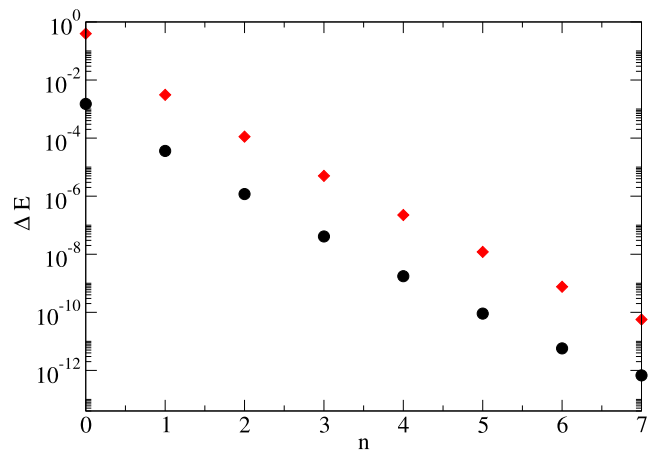


FIG. 9. Convergence of the energy as a function of photon spaces. $\omega = 0.1$ and $\lambda = (0.1, 0.1)$ are used in the calculations. ΔE is the difference between the energy calculated using $0, \dots, n$ photon spaces and the converged energy, which is calculated using photon spaces up to $n = 20$. The circles show the ground state; the diamond shows the first excited state.

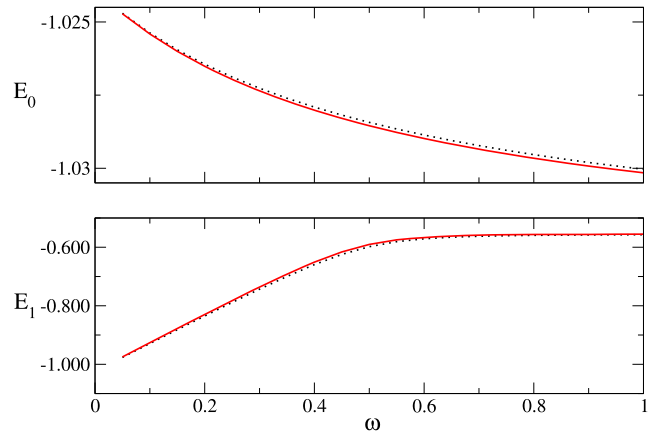


FIG. 10. Ground (E_0) and excited state (E_1) energies as a function of omega. The black solid line is calculated using n up to 20; the red dotted line is calculated using $n = 0$ and $n = 1$. $\lambda = (0.1, 0.1)$ is used in the calculations.

TABLE I. Ground and excited state energies of the 2D H_2^+ ion. $\omega = 0.1$ is used.

| Positions | $n = 0, \lambda = 0$ | $n = 0, \lambda = 0.1$ | $n < 2, \lambda = 0.1$ | $n < 5, \lambda = 0.1$ | $n < 10, \lambda = 0.1$ |
|-------------------|--------------------------------|--------------------------------|--------------------------------|--------------------------------|--------------------------------|
| (0,1/2), (0,-1/2) | -1.033 437 78 -0.558 280 08 | -1.023 907 03 -0.534 805 32 | -1.025 375 11 -0.926 062 92 | -1.025 411 20 -0.929 142 31 | -1.025 411 20 -0.929 142 53 |
| (1,1/2), (1,-1/2) | -1.033 437 78 -0.558 280 07 | -1.019 255 47 -0.530 772 89 | -1.024 904 32 -0.917 245 89 | -1.025 411 11 -0.929 133 83 | -1.025 411 20 -0.929 142 53 |

APPENDIX E: CONVERGENCE TESTS

In QED-HF,⁷¹ the energy is minimized with respect to the photon coefficients for a given Hartree–Fock state. In that case, the resulting energy [see Eq. (31) in Ref. 71] will be independent of the photon frequency ω . The aim of the Appendix is to numerically show that the energy calculated by the present approach remains ω dependent and that the energy does not depend on the position of the molecules with respect to the origin. The energy is ω dependent because our starting ansatz is a sum of products of spatial and photon states, and it cannot be factorized into a single product of spatial and photon functions similar to that in Ref. 71.

We will use a 2D model system to test the dependence of the energy on ω and on the position of the atoms with respect to the origin. The 2D representation allows exact diagonalization and a stringent numerical test. The model uses a H_2^+ ion with one electron and two protons at (0,1/2) and (0,-1/2), described with soft Coulomb potential (to avoid the singularity of the Coulomb potential in a grid representation). The electronic Hamiltonian is defined as

$$H_e = -\frac{\hbar^2}{2m} \left(\frac{d^2}{dx^2} + \frac{d^2}{dy^2} \right) - \frac{1}{\sqrt{x^2 + (y - 1/2)^2 + 1}} - \frac{1}{\sqrt{x^2 + (y + 1/2)^2 + 1}}. \quad (\text{E1})$$

We use a 100×100 grid with 0.2 grid spacing. This gives well-converged energies up to 8 decimal places.

Figure 9 shows the convergence of the energy of the ground and the first excited states when the number of photon spaces is increased. The energy converges very quickly in the $0 + 1$ photon spaces, and further enlargement of the photon space dimension does not significantly change the results. The same is true for the energy of the molecules calculated in this work, but full convergence tests up to high n states is prohibitively expensive in those cases.

Figure 10 shows that the energies depend on ω . The energies calculated using the lowest photon spaces ($n = 0$ and $n = 1$) show nearly identical dependence to the fully converged results (using n up to 20). Note that the dependence of the total energy in the TDDFT calculation is a sum of the orbital energies as a function of ω .

Finally, we have shifted the Coulomb centers (0,1/2) and (0,-1/2) with a (1,0) vector to test the dependence of the energy on the origin. Table I shows that this shift does not change the energy of the electronic states [$\lambda = (0,0)$ and $n = 0$]. Keeping $n = 0$ and using $\lambda = (0.1,0.1)$ changes the energies due the addition of the dipole self-interaction. In this case, the energy of the shifted system is different

from the original system, because the dipole self-interaction depends on the position. By increasing the number of photon spaces used in the calculation, this difference decreases and disappears if high enough bases are used (see Table I).

REFERENCES

- J. A. Hutchison, T. Schwartz, C. Genet, E. Devaux, and T. W. Ebbesen, *Angew. Chem., Int. Ed.* **51**, 1592 (2012).
- R. Balili, V. Hartwell, D. Snoke, L. Pfeiffer, and K. West, *Science* **316**, 1007 (2007).
- J. Schachenmayer, C. Genes, E. Tignone, and G. Pupillo, *Phys. Rev. Lett.* **114**, 196403 (2015).
- B. Xiang, R. F. Ribeiro, M. Du, L. Chen, Z. Yang, J. Wang, J. Yuen-Zhou, and W. Xiong, *Science* **368**, 665 (2020).
- A. Reserbat-Plantey, I. Epstein, I. Torre, A. T. Costa, P. A. D. Gonçalves, N. A. Mortensen, M. Polini, J. C. W. Song, N. M. R. Peres, and F. H. L. Koppens, *ACS Photonics* **8**, 85 (2021).
- D. M. Coles, N. Somaschi, P. Michetti, C. Clark, P. G. Lagoudakis, P. G. Savvidis, and D. G. Lidzey, *Nat. Mater.* **13**, 712 (2014).
- J. Kasprzak, M. Richard, S. Kundermann, A. Baas, P. Jeambrun, J. M. J. Keeling, F. M. Marchetti, M. H. Szymańska, R. André, J. L. Staehli *et al.*, *Nature* **443**, 409 (2006).
- T. Schwartz, J. A. Hutchison, C. Genet, and T. W. Ebbesen, *Phys. Rev. Lett.* **106**, 196405 (2011).
- J. D. Plumhof, T. Stöferle, L. Mai, U. Scherf, and R. F. Mahrt, *Nat. Mater.* **13**, 247 (2014).
- J. A. Hutchison, A. Liscio, T. Schwartz, A. Canaguier-Durand, C. Genet, V. Palermo, P. Samori, and T. W. Ebbesen, *Adv. Mater.* **25**, 2481 (2013).
- K. Wang, M. Seidel, K. Nagarajan, T. Chervy, C. Genet, and T. Ebbesen, *Nat. Commun.* **12**, 1486 (2021).
- D. N. Basov, A. Asenjo-Garcia, P. J. Schuck, X. Zhu, and A. Rubio, *Nanophotonics* **10**, 549 (2021).
- J. Feist and F. J. Garcia-Vidal, *Phys. Rev. Lett.* **114**, 196402 (2015).
- O. Vendrell, *Phys. Rev. Lett.* **121**, 253001 (2018).
- C. Schäfer and G. Johansson, *Phys. Rev. Lett.* **128**, 156402 (2022).
- R. R. Riso, T. S. Haugland, E. Ronca, and H. Koch, *Nat. Commun.* **13**, 1368 (2022).
- P. Badankó, O. Umarov, C. Fábri, G. J. Halász, and A. Vibók, *Int. J. Quantum Chem.* **122**, e26750 (2022).
- G. Mazza and A. Georges, *Phys. Rev. Lett.* **122**, 017401 (2019).
- O. Di Stefano, A. Settimeri, V. Macrì, L. Garziano, R. Stassi, S. Savasta, and F. Nori, *Nat. Phys.* **15**, 803 (2019).
- J. Galego, F. J. Garcia-Vidal, and J. Feist, *Phys. Rev. X* **5**, 041022 (2015).
- F. Herrera and F. C. Spano, *Phys. Rev. Lett.* **116**, 238301 (2016).
- J. Galego, F. J. Garcia-Vidal, and J. Feist, *Nat. Commun.* **7**, 13841 (2016).
- A. Shalabney, J. George, J. Hutchison, G. Pupillo, C. Genet, and T. W. Ebbesen, *Nat. Commun.* **6**, 5981 (2015).
- F. Buchholz, I. Theophilou, S. E. B. Nielsen, M. Ruggenthaler, and A. Rubio, *ACS Photonics* **6**, 2694 (2019).
- C. Schäfer, M. Ruggenthaler, H. Appel, and A. Rubio, *Proc. Natl. Acad. Sci. U. S. A.* **116**, 4883 (2019).

- ²⁶M. Ruggenthaler, N. Tancogne-Dejean, J. Flick, H. Appel, and A. Rubio, *Nat. Rev. Chem.* **2**, 0118 (2018).
- ²⁷J. Flick, M. Ruggenthaler, H. Appel, and A. Rubio, *Proc. Natl. Acad. Sci. U. S. A.* **112**, 15285 (2015).
- ²⁸J. Flick, M. Ruggenthaler, H. Appel, and A. Rubio, *Proc. Natl. Acad. Sci. U. S. A.* **114**, 3026 (2017).
- ²⁹L. Lacombe, N. M. Hoffmann, and N. T. Maitra, *Phys. Rev. Lett.* **123**, 083201 (2019).
- ³⁰A. Mandal, S. Montillo Vega, and P. Huo, *J. Phys. Chem. Lett.* **11**, 9215 (2020).
- ³¹J. Flick, D. M. Welakuh, M. Ruggenthaler, H. Appel, and A. Rubio, *ACS Photonics* **6**, 2757 (2019).
- ³²S. Latini, E. Ronca, U. De Giovannini, H. Hübener, and A. Rubio, *Nano Lett.* **19**, 3473 (2019).
- ³³J. Flick, N. Rivera, and P. Narang, *Nanophotonics* **7**, 1479 (2018).
- ³⁴J. Flick and P. Narang, *Phys. Rev. Lett.* **121**, 113002 (2018).
- ³⁵F. J. Garcia-Vidal, C. Ciuti, and T. W. Ebbesen, *Science* **373**, eabd0336 (2021).
- ³⁶A. Thomas, L. Lethuillier-Karl, K. Nagarajan, R. M. A. Vergauwe, J. George, T. Chervy, A. Shalabney, E. Devaux, C. Genet, J. Moran, and T. W. Ebbesen, *Science* **363**, 615 (2019).
- ³⁷U. Mordovina, C. Bunney, H. Appel, P. J. Knowles, A. Rubio, and F. R. Manby, *Phys. Rev. Res.* **2**, 023262 (2020).
- ³⁸D. S. Wang, T. Neuman, J. Flick, and P. Narang, *J. Chem. Phys.* **154**, 104109 (2021).
- ³⁹A. E. DePrince, *J. Chem. Phys.* **154**, 094112 (2021).
- ⁴⁰T. S. Haugland, C. Schäfer, E. Ronca, A. Rubio, and H. Koch, *J. Chem. Phys.* **154**, 094113 (2021).
- ⁴¹N. M. Hoffmann, L. Lacombe, A. Rubio, and N. T. Maitra, *J. Chem. Phys.* **153**, 104103 (2020).
- ⁴²J. Flick and P. Narang, *J. Chem. Phys.* **153**, 094116 (2020).
- ⁴³A. Mandal, T. D. Krauss, and P. Huo, *J. Phys. Chem. B* **124**, 6321 (2020).
- ⁴⁴J. Gallego, F. J. Garcia-Vidal, and J. Feist, *Phys. Rev. Lett.* **119**, 136001 (2017).
- ⁴⁵J. Flick, C. Schäfer, M. Ruggenthaler, H. Appel, and A. Rubio, *ACS Photonics* **5**, 992 (2018).
- ⁴⁶C. Schafer, M. Ruggenthaler, and A. Rubio, *Phys. Rev. A* **98**, 043801 (2018).
- ⁴⁷D. Sidler, M. Ruggenthaler, H. Appel, and A. Rubio, *J. Phys. Chem. Lett.* **11**, 7525 (2020).
- ⁴⁸I. Theophilou, M. Penz, M. Ruggenthaler, and A. Rubio, *J. Chem. Theory Comput.* **16**, 6236 (2020).
- ⁴⁹D. Sidler, C. Schäfer, M. Ruggenthaler, and A. Rubio, *J. Phys. Chem. Lett.* **12**, 508 (2021).
- ⁵⁰F. Buchholz, I. Theophilou, K. J. H. Giesbertz, M. Ruggenthaler, and A. Rubio, *J. Chem. Theory Comput.* **16**, 5601 (2020).
- ⁵¹I. V. Tokatly, *Phys. Rev. B* **98**, 235123 (2018).
- ⁵²N. Rivera, J. Flick, and P. Narang, *Phys. Rev. Lett.* **122**, 193603 (2019).
- ⁵³T. Szidarovszky, G. J. Halász, and Á. Vibók, *New J. Phys.* **22**, 053001 (2020).
- ⁵⁴L. S. Cederbaum, *J. Phys. Chem. Lett.* **12**, 6056 (2021).
- ⁵⁵D. Cho, B. Gu, and S. Mukamel, *J. Am. Chem. Soc.* **144**, 7758 (2022).
- ⁵⁶F. Pavošević and A. Rubio, *J. Chem. Phys.* **157**, 094101 (2022).
- ⁵⁷F. Pavošević and J. Flick, *J. Phys. Chem. Lett.* **12**, 9100 (2021).
- ⁵⁸F. Pavošević, S. Hammes-Schiffer, A. Rubio, and J. Flick, *J. Am. Chem. Soc.* **144**, 4995 (2022).
- ⁵⁹L. S. Cederbaum and A. I. Kuleff, *Nat. Commun.* **12**, 4083 (2021).
- ⁶⁰T. W. Ebbesen, *Acc. Chem. Res.* **49**, 2403 (2016).
- ⁶¹C. Genet, J. Faist, and T. W. Ebbesen, *Phys. Today* **74**(5), 42 (2021).
- ⁶²D. Sidler, M. Ruggenthaler, C. Schäfer, E. Ronca, and A. Rubio, *J. Chem. Phys.* **156**, 230901 (2022).
- ⁶³T. E. Li, B. Cui, J. E. Subotnik, and A. Nitzan, *Annu. Rev. Phys. Chem.* **73**, 43 (2022).
- ⁶⁴M. Sánchez-Barquilla, A. I. Fernández-Domínguez, J. Feist, and F. J. García-Vidal, *ACS Photonics* **9**, 1830 (2022).
- ⁶⁵J. Fregoni, F. J. García-Vidal, and J. Feist, *ACS Photonics* **9**, 1096 (2022).
- ⁶⁶E. T. Jaynes and F. W. Cummings, “Comparison of quantum and semiclassical radiation theories with application to the beam maser,” *Proc. IEEE* **51**(1), 89–109 (1962).
- ⁶⁷V. Rokaj, D. M. Welakuh, M. Ruggenthaler, and A. Rubio, *J. Phys. B: At., Mol. Opt. Phys.* **51**, 034005 (2018).
- ⁶⁸A. Ahrens, C. Huang, M. Beutel, C. Covington, and K. Varga, *Phys. Rev. Lett.* **127**, 273601 (2021).
- ⁶⁹M. Beutel, A. Ahrens, C. Huang, Y. Suzuki, and K. Varga, *J. Chem. Phys.* **155**, 214103 (2021).
- ⁷⁰M. D. Liebenthal, N. Vu, and A. E. DePrince, *J. Chem. Phys.* **156**, 054105 (2022).
- ⁷¹T. S. Haugland, E. Ronca, E. F. Kjønstad, A. Rubio, and H. Koch, *Phys. Rev. X* **10**, 041043 (2020).
- ⁷²J. Mitroy, S. Bubin, W. Horiuchi, Y. Suzuki, L. Adamowicz, W. Cencek, K. Szalewicz, J. Komasa, D. Blume, and K. Varga, *Rev. Mod. Phys.* **85**, 693 (2013).
- ⁷³M. Ruggenthaler, J. Flick, C. Pellegrini, H. Appel, I. V. Tokatly, and A. Rubio, *Phys. Rev. A* **90**, 012508 (2014).
- ⁷⁴I. V. Tokatly, *Phys. Rev. Lett.* **110**, 233001 (2013).
- ⁷⁵C. Pellegrini, J. Flick, I. V. Tokatly, H. Appel, and A. Rubio, *Phys. Rev. Lett.* **115**, 093001 (2015).
- ⁷⁶C. Schafer, F. Buchholz, M. Penz, M. Ruggenthaler, and A. Rubio, *Proc. Natl. Acad. Sci. U. S. A.* **118**, e2110464118 (2021).
- ⁷⁷J. Flick, “Simple exchange-correlation energy functionals for strongly coupled light-matter systems based on the fluctuation-dissipation theorem,” *Phys. Rev. Lett.* **129**, 143201 (2021).
- ⁷⁸J. Yang, Q. Ou, Z. Pei, H. Wang, B. Weng, Z. Shuai, K. Mullen, and Y. Shao, *J. Chem. Phys.* **155**, 064107 (2021).
- ⁷⁹L. Mandel, *Opt. Lett.* **4**, 205 (1979).
- ⁸⁰E. Runge and E. K. U. Gross, *Phys. Rev. Lett.* **52**, 997 (1984).
- ⁸¹N. Troullier and J. L. Martins, *Phys. Rev. B* **43**, 1993 (1991).
- ⁸²M. A. D. Taylor, A. Mandal, and P. Huo, *Opt. Lett.* **47**, 1446 (2022).
- ⁸³J. R. Chelikowsky, N. Troullier, and Y. Saad, *Phys. Rev. Lett.* **72**, 1240 (1994).
- ⁸⁴K. Yabana and G. F. Bertsch, *Phys. Rev. B* **54**, 4484 (1996).
- ⁸⁵N. Tancogne-Dejean, M. J. T. Oliveira, X. Andrade, H. Appel, C. H. Borca, G. Le Breton, F. Buchholz, A. Castro, S. Corni, A. A. Correa *et al.*, *J. Chem. Phys.* **152**, 124119 (2020).
- ⁸⁶K. Varga, Z. Zhang, and S. T. Pantelides, *Phys. Rev. Lett.* **93**, 176403 (2004).
- ⁸⁷J. Gallego, C. Climent, F. J. Garcia-Vidal, and J. Feist, *Phys. Rev. X* **9**, 021057 (2019).
- ⁸⁸F. Benz, M. K. Schmidt, A. Dreismann, R. Chikkaraddy, Y. Zhang, A. Demetriadiou, C. Carnegie, H. Ohadi, B. de Nijs, R. Esteban *et al.*, *Science* **354**, 726 (2016).
- ⁸⁹C. Carnegie, J. Griffiths, B. de Nijs, C. Readman, R. Chikkaraddy, W. M. Deacon, Y. Zhang, I. Szabó, E. Rosta, J. Aizpurua, and J. J. Baumberg, *J. Phys. Chem. Lett.* **9**, 7146 (2018).
- ⁹⁰J. D. Mallory and A. E. DePrince, “Reduced-density-matrix-based ab initio cavity quantum electrodynamics,” [arXiv:2204.00725](https://arxiv.org/abs/2204.00725) (2022).
- ⁹¹A. D. Becke, *J. Chem. Phys.* **140**, 18A301 (2014).
- ⁹²F. Caruso, D. R. Rohr, M. Hellgren, X. Ren, P. Rinke, A. Rubio, and M. Scheffler, *Phys. Rev. Lett.* **110**, 146403 (2013).
- ⁹³A. F. Kockum, V. Macri, L. Garziano, S. Savasta, and F. Nori, *Sci. Rep.* **7**, 5313 (2017).
- ⁹⁴T. Chervy, J. Xu, Y. Duan, C. Wang, L. Mager, M. Frerejean, J. A. W. Münnighoff, P. Tinnemanns, J. A. Hutchison, C. Genet *et al.*, *Nano Lett.* **16**, 7352 (2016).
- ⁹⁵F. Barachati, J. Simon, Y. A. Getmanenko, S. Barlow, S. R. Marder, and S. Kéna-Cohen, *ACS Photonics* **5**, 119 (2018).
- ⁹⁶B. Liu, M. Crescimanno, R. J. Twieg, and K. D. Singer, *Adv. Opt. Mater.* **7**, 1801682 (2019).
- ⁹⁷D. M. Welakuh and P. Narang, “Tunable nonlinearity and efficient harmonic generation from a strongly coupled light-matter system,” [arXiv:2203.00691](https://arxiv.org/abs/2203.00691) (2022).
- ⁹⁸V. A. Goncharov and K. Varga, *J. Chem. Phys.* **137**, 094111 (2012).
- ⁹⁹C. A. Ullrich, *Time-Dependent Density-Functional Theory: Concepts and Applications* (Oxford University Press, 2012).